

On the formation of molecules and solid-state compounds from the AGB to the PN phases

D. A. García-Hernández^{1,2} and A. Manchado^{1,2,3}

¹ Instituto de Astrofísica de Canarias, C/ Via Láctea s/n, E-38205 La Laguna, Spain

² Departamento de Astrofísica, Universidad de La Laguna (ULL), E-38206 La Laguna, Spain

³ Consejo Superior de Investigaciones Científicas, Spain

E-mail: agarcia@iac.es; amt@iac.es

Abstract. During the asymptotic giant branch (AGB) phase, different elements are dredge-up to the stellar surface depending on progenitor mass and metallicity. When the mass loss increases at the end of the AGB, a circumstellar dust shell is formed, where different (C-rich or O-rich) molecules and solid-state compounds are formed. These are further processed in the transition phase between AGB stars and planetary nebulae (PNe) to create more complex organic molecules and inorganic solid-state compounds (e.g., polycyclic aromatic hydrocarbons, fullerenes, and graphene precursors in C-rich environments and oxides and crystalline silicates in O-rich ones). We present an observational review of the different molecules and solid-state materials that are formed from the AGB to the PN phases. We focus on the formation routes of complex fullerene (and fullerene-based) molecules as well as on the level of dust processing depending on metallicity.

1. Introduction

Low- and intermediate-mass ($1 < M < 8 M_{\odot}$) stars suffer strong mass loss and a series of thermal pulses at the tip of the asymptotic giant branch (AGB) phase. The interstellar medium (ISM) is thus efficiently enriched with specific elements/isotopes and dust grains expelled by AGB stars. The principal nucleosynthetic processes occur on the thermal pulsing (TP) AGB phase, while the main molecular/dust processing takes place during the short transition phase between the AGB phase and the planetary nebula (PN) stage. Carbon (^{12}C) and s-process neutron-rich elements (e.g., Rb, Zr, Sr, Nd, Ba, Tc) are synthesized and transported to the stellar surface during the TP-AGB phase. Solar metallicity low-mass ($M < 1.5 M_{\odot}$) AGB stars remain O-rich and they probably do not form an observable PN, while more massive ($1.5 < M < 4 M_{\odot}$) AGBs are converted to C-rich ($\text{C}/\text{O} > 1$) stars. The most massive ($M > 4 M_{\odot}$) AGBs remain also as O-rich stars because of the activation of the hot bottom burning (HBB) process. Also, the dominant neutron source (^{13}C vs. ^{22}Ne) at the s-process site depends on stellar mass, which translates into different s-process abundances patterns (e.g., the $[\text{Rb}/\text{Zr}]$ ratio; see e.g., [1]). This basic AGB picture is strongly dependent on metallicity (e.g., [1,2,3] and references therein); e.g., the minimum progenitor mass to efficiently activate the HBB process decreases at lower metallicities. The higher mass AGB stars thus produce different elements/isotopes than the lower mass AGB ones, this being imprinted in the gas and circumstellar dust chemistry. At the end of the AGB, the more massive C-rich and O-rich stars are also heavily obscured by their thick circumstellar

dust envelopes (CSE), experiencing a phase of total obscuration in their way to form PNe; they are thus only accessible in the infrared (IR) and millimeter spectral ranges.

AGB and post-AGB stars are also amazing molecular factories; i.e., more than 70 molecules have been detected in AGB CSE through their rotational transitions from the IR to millimeter wavelengths (e.g., [4]). These are mainly gas-phase molecules: i), inorganics like SiS and AlCl; ii) organics such as H₂CO and CH₃CN; iii) radicals (e.g., HCO⁺); iv) rings (e.g., C₃H₂); and v) chains (e.g., HC₉N). We note that the formation of most (although not all) of these molecules may be explained by gas-phase reactions but solid-state chemistry has to be considered also in the models; i.e., molecules (e.g., H₂) may form on dust grains.

The CSE dust composition of sources evolving from the AGB to the PN stage depends on the dominant star's chemistry (i.e., the C/O ratio). The C-rich (C/O>1) AGB stars show SiC and amorphous carbon, although other complex and disordered organic solids with mixed aromatic/aliphatic structures like kerogen and coal may provide also the strong dust continuum emission (e.g., [5]). The O-rich (C/O<1) AGBs, however, display amorphous silicates, weak crystalline silicates such as piroxenes, and refractory oxides (e.g., corundum and spinel) (e.g., [6]). On the other hand, young and evolved O-rich PNe mainly display strong crystalline silicate features, while the aromatic infrared bands (AIBs, generally attributed to polycyclic aromatic hydrocarbons; PAHs) and unidentified IR emission features (UIRs) are observed in the C-rich ones. Finally, double-chemistry PNe are characterized by both C-rich (e.g., PAHs) and O-rich (e.g., crystalline silicates) dust features (e.g., [7]).

Several dust types can be differentiated depending on the solid-state features observed in the *Spitzer Space Telescope* spectroscopic observations of Galactic PNe (see Figure 1, left panel), which otherwise are generally characterized by a strong IR dust continuum emission [8,9]. Carbon chemistry (CC) and oxygen chemistry (OC) PNe display respectively C-rich and O-rich dust features that may be aliphatic/amorphous and/or aromatic/crystalline. Double-chemistry (DC) PNe simultaneously show C-rich (mainly aromatic) and O-rich dust features (crystalline and/or amorphous). Finally, featureless (F) PNe show only nebular emission lines in their IR spectra with very weak dust continuum emission.

In general, there is a process of crystallization or aromatization during the short ($\sim 10^2$ - 10^4 years) transition phase AGB–PN and the crystalline (O-rich) and aromatic (C-rich) structures are created during this short stage (e.g., [10,5,11]). Stars evolving from AGB stars to PNe are thus great laboratories for astrochemistry, providing us with strong observational constraints on the gas-phase and solid-state chemical models. The major challenge is to unveil the formation routes of these complex organic molecules and inorganic solid-state compounds. Here we present an observational review of the several molecular (and solid-state) materials that are formed in the AGB–PN phase, focussing on the formation pathways of complex fullerene (and fullerene-based) molecules as well as on the level of dust processing depending on metallicity.

2. Dust composition versus metallicity

The different *Spitzer* dust types observed in PNe are shown in Figure 1 (left panel). These *Spitzer* dust types show a strong dependence on metallicity; see Table 1 in [12] where the *Spitzer* dust type statistics for Galactic bulge (high metallicity) and disk (intermediate metallicity) PNe are compared with those observed in the lower metallicity PNe of the Magellanic Clouds (MCs). Dust features overimposed to the dust continuum are less frequent at the lower MC metallicities. Crystalline silicate features (and another O-rich dust features) are quite rare in the MCs, where carbon chemistry (CC) PNe are predominant [13]. In addition, double-chemistry (DC) PNe dominate towards the Galactic bulge [7], while they are not observed in the low-metallicity environments of the MCs. The mixed-chemistry (DC), C-rich (CC), and O-rich (OC) PNe are equally distributed in the Galactic disk [8,9].

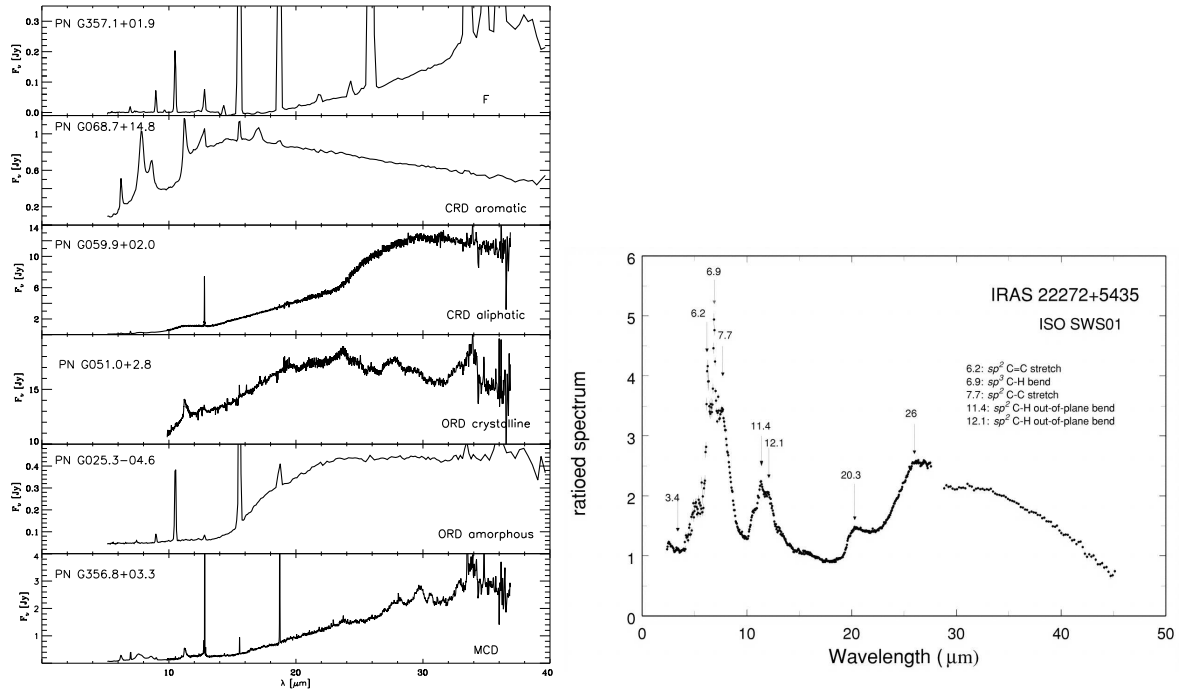


Figure 1. Left panel: Examples of the several *Spitzer* dust types found in compact (presumably young) Galactic PNe; from top to bottom: featureless (F); carbon-chemistry aromatic or aliphatic (CCar or CCal); oxygen-chemistry crystalline or amorphous (OCcr or OCam); and double-chemistry (DC) (updated from [8]). Right panel: Infrared Space Observatory (ISO) spectrum of the proto-PN IRAS 22272+5435 showing the presence of the still unidentified 21, 26, and 30 μm features (updated from [14]). The aliphatic discrete features (e.g., at 3.4 and 6.9 μm) and the 8 and 12 μm aliphatic plateaus together with AIBs (e.g., at 6.2 and 7.7 μm) are also seen.

2.1. Oxygen-rich dust PNe

The O-rich dust PNe are less frequent at the lower MC metallicities [13] and the several *Spitzer* O-dust subtypes (amorphous or crystalline) vary with metallicity (e.g., [9]). In particular, the $\sim 9.7 \mu\text{m}$ broad emission band due to amorphous silicates is more common in the Galactic disk (intermediate metallicity), while the narrower crystalline silicate emission features (such as those of olivine and pyroxene at ~ 23.5 , 27.5 , and $33.5 \mu\text{m}$) completely dominate in the Galactic bulge (high metallicity), which otherwise are almost absent in the MCs. The O-rich dust features evolve from amorphous to crystalline silicates during the AGB–PN phase [10]. Two main scenarios may explain the silicates crystallization depending on temperature: a) at low temperature in long-lived circumbinary disks [15]; or b) at high temperature, because of the strong mass loss, at the tip of the AGB [6].

2.2. Carbon-rich dust PNe

A different situation is found for the C-rich dust PNe. They are more common at the low metallicity of the MCs than at higher metallicity (Galactic disk or bulge). In the MCs, the C-rich dust PNe generally display small dust grains (or less processed) [13]; the C-rich aliphatic dust features dominate their *Spitzer* spectra, while the PAH-like emission bands are very rare. In addition, the C-rich dust PNe dominate at the MC low-metallicity but they are not observed at the very high metallicity of the Galactic bulge. In particular, broad emission dust features of

aliphatic character (e.g., at ~ 9 – 13 , 15 – 20 , and 25 – 35 μm ; see Section 3) are usually detected in MC PNe, while Galactic disk C-rich dust PNe are usually compact (presumably young) PNe of slightly subsolar metallicity [9]. In the case of nearly solar metallicities, small hydrocarbon molecules (e.g., acetylene) are synthesized in the short transition phase AGB–PN, replacing the broad $\sim 11.5\mu\text{m}$ feature due to SiC (as well as the strong dust continuum emission) seen in the previous AGB phase. The IR features rapidly change from aliphatic to PAH-like (aromatic) during the post-AGB phase and the nebular emission lines (sometimes the broad ~ 25 – 35 μm aliphatic emission feature is still detected) prevail in the PN stage [10]. The level of dust processing seems to vary with the metallicity of the environment. For example, the transition from aliphatic structures (the ~ 9 – 13 , 15 – 20 , and 25 – 35 μm features) to aromatic ones (the 6.2 , 7.7 , 8.6 , and 11.3 μm PAH-like features) proceeds more slowly at the MCs metallicity [13]. Two models for the aromatization process from AGB stars to PNe have been proposed: a) the PAH precursors are acetylene (C_2H_2) and its radical derivatives [16]; or b) the PAHs are formed as a consequence of the photochemical processing of the dust grains, which transform aliphatics to aromatics (e.g., [14,10]).

3. Unidentified infrared emission features at 21, 26, and 30 μm

The still unidentified set of IR emission features at ~ 21 , 26 , and 30 μm is observed in C-rich sources evolving from AGB stars to PNe (see Figure 1, right panel).

The carrier of the 21 μm feature, generally observed in post-AGB stars, should be a fragile solid-state carbon compound (e.g., [17]). Several carriers such as hydrogenated fullerenes, TiC nanoclusters, nanodiamonds, HAC, and amides have been proposed in the literature but we still lack a firm identification.

The 30 μm feature (sometimes with substructure at ~ 26 μm), however, has been linked with magnesium sulfide [18], aliphatic chains [19] or HACs [20]. The carrier should be quite abundant in the CSE because it is detected from the AGB to the PN phases, carrying out a significant fraction of the total energy output. Remarkably, the HAC-like identification, some kind of solid with a mixed aromatic/aliphatic structure that may also explain the 21 and 26 μm features [20], could explain the formation of complex dehydrogenated organics like C_{60} , C_{70} , and planar C_{24} (a small piece of a graphene sheet) in some C-rich PNe (see below).

4. Detection of complex dehydrogenated molecules

Kroto et al. [21] discovered the tridimensional C_{60} and C_{70} fullerene molecules at laboratory and their high stability reinforced the hypothesis that they should be widespread in the ISM, being important species for the interstellar/circumstellar chemistry. These complex species may give an explanation to several phenomena in Astrophysics. For example, they may explain the diffuse interstellar bands (DIBs) (22; see e.g., [23] for a review on interstellar/circumstellar DIBs) and the UV bump (e.g., [24]). Fullerenes were indeed found on Earth and on meteorites and various unsuccessful fullerene searches (e.g., by using the Infrared Space Observatory) were made to find the four mid-IR features (at ~ 7.0 , 8.5 , 17.4 , and 18.9 μm ; see Figure 2, left panel) of the C_{60} fullerene towards proto-PNe (e.g., [25]) and R Coronae Borealis (RCB) stars (e.g., [26]).

Nowadays, C_{60} and C_{70} (first discovered in space by [27]¹) are known to be efficiently formed in H-rich circumstellar envelopes only [28,29]. Fullerenes are detected in low-mass C-rich PNe (both in the Milky Way and in the MCs) with normal H abundances [28,30] and in only those RCB stars with some H [29]; C_{60} is usually seen in conjunction with PAH-like features. Indeed,

¹ These authors interpreted the detection of C_{60} and C_{70} in the PN Tc 1 as due to the H-poor conditions in the inner core. This interpretation is in agreement with some laboratory experiments that show that fullerenes are efficiently produced under the absence of H. However, neither the central star, nor the inner core and the nebula are H-poor or H-deficient. Thus, current understanding of stellar astrophysics does not allow for Tc 1 being a H-poor (late TP) PN (see e.g., [28,29]).

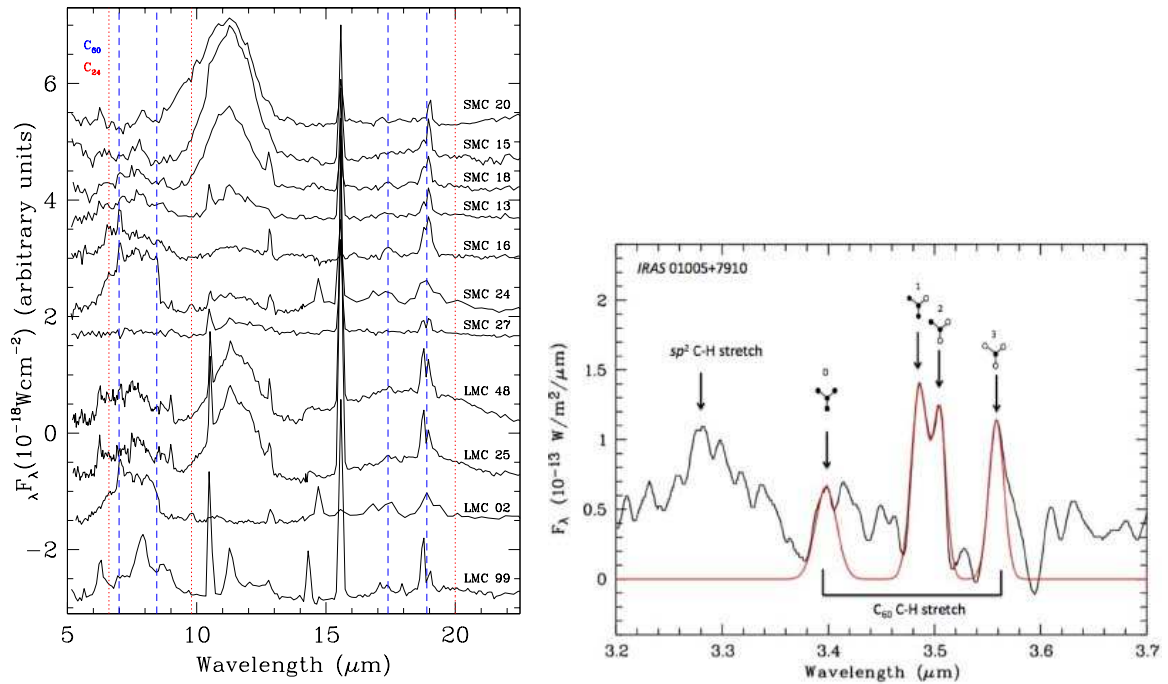


Figure 2. Left panel: *Spitzer* residual spectra of fullerene-containing PNe in the MCs. The band positions of C_{60} (dashed) and planar C_{24} (dotted) are marked (updated from [30]). Right panel: ISO spectrum of the PPN IRAS 01005+7910 in the 3-4 μm spectral region covering several fullerane features. Note the peaks for the 0, 1, 2, and 3 non-H-bonded neighboring carbon atoms that may be attributed to fullerenes (updated from [40]).

the C_{60} molecule has also been detected in another astronomical environments such as a PPN [31], reflection nebulae [32], and young stellar objects [33] and none of them is H-deficient.

Interestingly, unusual IR emission features at ~ 6.6 , 9.8 , and $20 \mu\text{m}$, attributed to the planar C_{24} molecule (a small piece of a graphene sheet), have been also detected in MC and Galactic PNe [30,34] and in the ISM [35]. Figure 2 (left panel) shows the planar C_{24} and C_{60} emission features detected in some PNe. The detection of several complex dehydrogenated organic molecules like fullerenes and possible planar C_{24} (in conjunction with aromatic species like PAHs) suggests that other forms of carbon such as hydrogenated fullerenes (fulleranes like $C_{60}H_{36}$ and $C_{60}H_{18}$), fullerene-PAHs adducts, metallofullerenes or even buckyonions and carbon nanotubes, may be widespread in the Universe. For example: i) the recent studies of DIBs in C_{60} -rich PNe [36,37] suggests the possibility that some DIB carrier molecules may represent other fullerene-related molecules like buckyonions; ii) laboratory spectroscopy of adducts between fullerenes and PAHs (e.g., C_{60} -anthracene/tetracene/pentacene) shows that such fullerene-PAHs species display the same mid-IR features of isolated C_{60} molecules, being non distinguishable through mid-IR spectroscopy only [38]; and iii) the recent non-detections of the most intense IR bands of several fulleranes in two fullerene PNe [39] together with the (tentative) fulleranes detection in the proto-PN IRAS 01005+7910 [40] (see also Figure 2, right panel) suggest that fulleranes may be formed in the short transition phase between AGB stars and PNe but they are quickly destroyed by the UV radiation field from the central star.

5. Formation routes of complex dehydrogenated organics

The formation process of fullerene and graphenic nanostructures in space is still unclear to date. Several fullerene formation mechanisms have been proposed, the most notable ones being: i) the formation in H-poor environments [41]; ii) high-temperature formation in C-rich environments [42]; iii) photochemical processing of hydrogenated amorphous carbon grains (HACs; [28]); and iv) photochemical processing of large PAHs [43]. The first two mechanisms prevent the formation of hydrogenated species, something that seems to be difficult to reconcile with the astronomical observations. The alternative top-down approaches involve the photochemical processing of HACs and large PAHs as first proposed by [28] and [43], respectively. Both formation scenarios are based on top-down chemical models towards the most stable C₆₀ and C₇₀ fullerenes. These top-down fullerene formation scenarios (enumerated below) seem to be quite different to the fullerene production methods usually employed on Earth. The terrestrial vaporization or combustion synthesis routes to form fullerene-like species cannot work in space due to the low gas densities in the astrophysical environments; e.g., at laboratory, the main formation channel for C₆₀ is the build-up from atomic C, C₂, small C clusters, and rings [44].

5.1. Photochemical processing of HAC-like materials

Remarkably, fullerene PNe display broad HAC-like dust features at $\sim 9\text{--}13$ and $25\text{--}35$ μm , suggesting that the most likely explanation for the simultaneous presence of fullerenes, (possibly) planar C₂₄, and PAH-like emission in the H-rich circumstellar envelopes of PNe is that these molecular species may be formed from the destruction (e.g., as a consequence of the UV radiation from the central star) of a carbonaceous compound with a mixture of aromatic and aliphatic structures - e.g., HACs - , which should be a major constituent in their circumstellar envelopes [28,30,34]. It is to be noted here that there are other carbonaceous materials with a mixture of aromatic and aliphatic structures similar to HACs. For example, the mixed aromatic/aliphatic organic nanoparticles (MAONs) first introduced by Prof. Sun Kwok (e.g., [45,46]). The closest natural analogue of such structure is probably kerogen, which are random arrays of aromatic rings and aliphatic chains with functional groups made up of H, N, O, and S attached and that may contribute to the solid-state mid-IR features detected in proto-PNe (e.g., [47]). The coexistence of a large variety of molecular species such as HACs, PAH clusters, fullerenes, and small dehydrogenated carbon clusters (possibly planar C₂₄ or graphene precursors) in PNe with fullerenes strongly supports the few laboratory experiments carried out by Scott and colleagues in the nineties, which showed that the decomposition of HACs is sequential with small dehydrogenated PAH molecules being released first, followed by fullerenes and large PAH clusters [48]. This fullerene formation scenario is also suggested by the strong - and unique - spectral variations (in a timescale of just a few years) seen in the IR spectrum of the fullerene-containing RCB star V854 Cen, which indicate that a significant fraction of the dust grains in the envelope have evolved from HACs to complex species such as PAHs and fullerene-like molecules [29]. The recent works by [49,50] also suggest that fullerene formation in PNe likely starts from HAC processing. Perhaps the most novel idea is introduced by [50] who propose that UV-photolysis produces structural changes in the HAC grains, forming 3D hollow structures or arophatic clusters (aromatic clusters linked by aliphatic bridging groups). These arophatic clusters end up with a cage-like, cup-like or tube-like aspect, being curled-up or folded-over graphene sheets. Further UV-induced dehydrogenation of these arophatic clusters may introduce pentagonal rings, permitting the curvature of the structure into large fullerene cages that can shrink down to the most stable C₆₀ and C₇₀ fullerene configurations.

5.2. Photochemical processing of large PAHs

This fullerene formation route has been proposed to explain the formation of fullerenes in the ISM [43]. These authors propose an alternative top-down model where large PAHs (with ~ 70

C atoms) are converted into graphene, and subsequently fullerenes, under the action of UV photons from massive stars. A schematic view of this alternative top-down fullerene formation model is shown in Figure 3 of [43]. Upon UV irradiation, graphene formation takes place through PAH photolysis. The expected dehydrogenation, fragmentation, and isomerization can give rise to a rich organic chemistry, forming fullerenes, small cages, rings, and chains. Carbon loss followed by pentagonal defects formation that induces curvature of the graphene sheet may form fullerenes by migration of the pentagons. Remarkably, planar molecules such as C_{20} - C_{30} are expected to be formed by further graphene fragmentation. In the reflection nebula NGC 7023, emission at $6.6 \mu\text{m}$ (attributed to possible planar C_{24} molecules) is seen near the ionizing star [35], suggesting that the carrier is a photo-product of PAHs. In this context, the possible detection of the very stable planar C_{24} molecule in the ISM is also consistent with the idea of fullerene production from the photochemical processing of PAHs via graphene formation.

6. Complex dehydrogenated organics versus metallicity

Interestingly, the detection rate of complex dehydrogenated fullerene molecules in C-rich PNe decreases with increasing metallicity. In our own Galaxy, only $\sim 5\%$ of the PNe display the fullerene features, which otherwise are clearly detected in $\sim 20\%$ and $\sim 44\%$ of the PNe observed in the LMC and SMC, respectively [34]. This interesting finding suggests a higher presence of small dust grains (or a more limited dust processing) at the lower MCs metallicity. More recently, [51] demonstrate that all Galactic fullerene-containing PNe are low-mass objects of sub-solar metallicity, showing that low metallicity environments are more favourable to fullerene production and detection.

On the other hand, the still unidentified $21 \mu\text{m}$ feature is less frequent in the Galaxy than in the MCs [52] and the $21 \mu\text{m}$ carrier could be related with the formation of fullerenes. In particular, an anti-correlation between the $30 \mu\text{m}$ and other UIR features is seen among the $21 \mu\text{m}$ sources in the MCs [52] and such anti-correlation could result from the photochemical processing of HAC-like dust grains into fullerenes and PAHs. Under the HACs hypothesis for fullerene formation, the $21 \mu\text{m}$ feature should be related with the formation of fullerenes with the carrier being a fragile intermediate product from the decomposition of HAC or a similar material with mixed aromatic/aliphatic structures. However, [53], although based on a smaller sample of Galactic post-AGB stars, reported that the $30 \mu\text{m}$ feature and the other UIRs are not anti-correlated in Galactic $21 \mu\text{m}$ objects. Interestingly, the Galactic $21 \mu\text{m}$ emitters are spectroscopically different to the MC ones; i.e., the $21 \mu\text{m}$ proto-PNe in the MCs show more (typical) PAH-like aromatic features.

7. Concluding remarks

The IR dust characteristics (and evolution) observed from the AGB to the PN phases in different metallicity environments (Galactic disk, bulge, and MCs) agree well with the predictions of the AGB nucleosynthesis models (i.e., the expected effects of the third dredge-up and HBB processes). The coexistence of aromatic PAH-like species and complex dehydrogenated organic molecules such as fullerenes and planar C_{24} (a small piece of a graphene sheet) suggests a top-down model for the formation of fullerenes in space. Low metallicity environments like those of the MCs favour fullerene formation and detection as well as a more limited dust processing (or the general presence of small dust grains). Although more observational and laboratory efforts are needed, it seems clear that a diverse family of fullerene-related molecules (e.g., fullerenes, metallofullerenes, fullerene-PAH adducts, buckyonions, etc.) is very likely to be present in space.

Acknowledgments

D.A.G.H. was funded by the Ramón y Cajal fellowship number RYC–2013–14182. D.A.G.H and A. M. acknowledge support provided by the Spanish Ministry of Economy and Competitiveness

(MINECO) under grant AYA–2014–58082-P.

References

- [1] García-Hernández, D A et al. 2006 *Science* **314** 1751
- [2] García-Hernández, D A et al. 2007 *A&A* **462** 711
- [3] García-Hernández, D A et al. 2009 *ApJ* **705** L31
- [4] Herbst, E, vanDishoeck, E F 2009 *ARA&A* **47** 427
- [5] Kwok, S 2004 *Nature* **430** 985
- [6] Waters, L B F M et al. 1996 *A&A* **315** L361
- [7] Perea-Calderón, J V et al. 2009 *A&A* **495** L5
- [8] Stanghellini, L et al. 2012 *ApJ* **753** 172
- [9] García-Hernández, D A, Górnny, S K 2014 *A&A* **567** A12
- [10] García-Lario, P, Perea-Calderón, J V 2003 *ESA Publication Series* **511** 97
- [11] García-Hernández, D A 2012 in *IAU Symp. 283, Cambridge Univ. Press* **148**
- [12] García-Hernández, D A 2016 in *IAU GA XXIX, Cambridge Univ. Press (in press)* arXiv:1511.06165
- [13] Stanghellini, L et al. 2007 *ApJ* **671** 1669
- [14] Kwok, S et al. 2001 *ApJ* **554** L87
- [15] Molster, F J et al. 1999 *Nature* **401** 563
- [16] Cernicharo, J 2004, *ApJ* **608** L41
- [17] Volk, K, Kwok, S, Hrivnak, B J 1999 *ApJ* **516** L99
- [18] Hony, S et al. 2002 *A&A* **390** 533
- [19] Papoular, R 2011 *MNRAS* **415** 494
- [20] Grishko, V I et al. 2001 *ApJ* **558** L129
- [21] Kroto, H W et al. 1985 *Nature* **318** 162
- [22] Foing, B H, Ehrenfreund, P 1994 *Nature* **369** 296
- [23] Luna, R et al. 2008 *A&A* **480** 133
- [24] Iglesias-Groth, S 2004 *ApJ* **608** L37
- [25] Kwok, S et al. 1999 *A&A* **350** L35
- [26] Lambert, D L et al. 2001 *ApJ* **555** 925
- [27] Cami, J et al. 2010 *Science* **329** 1180
- [28] García-Hernández, D A et al. 2010 *ApJ* **724** L39
- [29] García-Hernández, D A, Rao, N K, Lambert, D L 2011 *ApJ* **729** 126
- [30] García-Hernández, D A et al. 2011 *ApJ* **737** L30
- [31] Zhang, Y, Kwok, S 2011 *ApJ* **730** 126
- [32] Sellgren, K 2010 *ApJ* **722** L54
- [33] Roberts, K R G, Smith, K T, Sarre, P J 2012 *MNRAS* **421** 3277
- [34] García-Hernández, D A et al. 2012 *ApJ* **760** 107
- [35] Berné, O, Mulas, G, Joblin, C 2013 *A&A* **550** L4
- [36] García-Hernández, D A, Díaz-Luis, J J 2013 *A&A* **550** L6
- [37] Díaz-Luis, J J et al. 2015 *A&A* **573** A97
- [38] García-Hernández, D A, Cataldo, F, Manchado, A 2013 *MNRAS* **434** 415
- [39] Díaz-Luis, J J et al. 2016 *A&A (in press)* arXiv:1602.07481
- [40] Zhang, Y, Kwok, S 2013 *EP&S* **65** 1069
- [41] Goeres, A, Sedlmayr, E 1992 *A&A* **265** 216
- [42] Jäger, C et al. 2009 *ApJ* **696** 706
- [43] Berné, O, Tielens, A G G M 2012 *PNAS* **109** 401
- [44] Heath, J R 1992 *J. Am. Chern. Soc.* **481** 1
- [45] Kwok, S, Zhang, Y 2011 *Nature* **479** 80
- [46] Zhang, Y, Kwok, S 2015 *ApJ* **798** 37
- [47] Cataldo, F, Keheyan, Y, Heymann, D 2002 *IJA* **1** 79
- [48] Scott, A et al. 1997 *ApJ* **489** L123
- [49] Bernard-Salas, J et al. 2012 *ApJ* **757** 41
- [50] Micelotta, E et al. 2012 *ApJ* **761** 35
- [51] Otsuka, M et al. 2014 *MNRAS* **437** 2577
- [52] Volk, K et al. 2011 *ApJ* **735** 127
- [53] Mishra, A, Li, A, Jiang, B W 2015 *ApJ* **802** 39